Preliminary Workflow for Subsurface Fracture Mapping Using 3D Seismic Surveys: A Case Study From the Cooper Basin, South Australia

Hani Abul Khair[1], Dennis Cooke[1], Rosalind King[2], Martin Hand[3], and Mark Tingay[1]

[1] Australian School of Petroleum, University of Adelaide, Australia
[2] School of Earth and Environmental Sciences, University of Adelaide, Australia
[3]SA Centre for Geothermal Energy Research, University of Adelaide, Australia

Keywords

Cooper Basin, curvature, ant tracks, fracture mapping, fracture susceptibility

Abstract

The future success of both enhanced (engineered) geothermal systems and shale gas production relies significantly on the development of reservoir stimulation strategies that suit the local stress and mechanical conditions of the prospects. The orientation and nature of the in-situ stress field and pre-existing natural fracture networks in the reservoir are amongst the critical parameters controlling the success of any stimulation program.

This work follows an initial study showing the existence of natural fractures in the area covered by the Moomba–Big Lake 3D seismic survey, in the South-Western termination of the Nappamerri Trough of the Cooper Basin in South Australia. The fractures, imaged both by borehole image logs and seismic attributes (Most Positive Curvature and Ant tracking), are pervasive across the seismic survey, and present a relatively constant NW-SE orientation.

We processed and analyzed the 3D seismic cube, Moomba-Big Lake survey in the Cooper Basin. Most positive curvature attribute (MPC) was then calculated from a structurally smoothed, non-steered version of the seismic cube.

Comparing the curvature signatures with the seismic amplitude signatures indicated that all the curvature values ≥ 0.2 are mapping structural features that enhance fracture stimulation (i.e. faults and folds). A new cube with curvature values ≥ 0.2 was then generated, and the ant tracking technique was applied to the final cube. We calibrated the resulting cube using seismic amplitudes, image logs, and well data and a highly positive correlation was found. Also, analysis shows that under present day stress orientation and magnitudes, fractures striking NW-SE and NE-SW are more susceptible to stimulation, and are more likely to open for fluid flow.

Accordingly, the current procedure provided a solution for mapping structural features pre-drilling, which affect reservoir porosity and permeability and will help developing stimulation strategies.

Introduction

Geothermal and unconventional development of naturally fractured reservoirs is significantly influenced by the characteristics of the fracture network, which controls the volume and flow direction of the gas and/or hot water through the hosting layers within unconventional and geothermal reservoirs, respectively. Detailed knowledge of fracture characteristics allows the design of well paths that intersect a larger number of permeable fractures, thus increasing production and enabling prediction of preferential flow paths. A good understanding of the fracture network in terms of intensity, orientation, and spatial distribution is therefore essential for both well planning and geothermal reservoir development. The key methods employed until now in fracture mapping can be summarized as follows:

- Core study and image log interpretation provide sparse fracture characterization on a small scale. These data are of high accuracy, but are only valid in the vicinity of the borehole, so extrapolation beyond the borehole might lead to erroneous prediction of the overall reservoir mechanics.
- Structural interpretation and structural basin models using seismic data describe faulting on a large scale and provide an idea of the overall stresses that initiated the structural features within the basin. This is used in some cases to address the general trend of the fractures rather than an actual measure of subsurface natural fracture network.
- Geomechanics, where a physical understanding of the fracturing process is combined with measurements of mechanical properties of rock to predict fracture network characteristics (Olson and Pollard, 1989; Rives et al., 1992; Lyakhovsky, 2001). The subcritical fracture index, a rock parameter that can be measured from core samples, is used to constrain the distributions of fracture aperture, spacing and length (Olson et al., 2001).

- Statistical modelling of fracture network geometry including two approaches. The first addresses each fracture characteristic separately and distributions are fit to the data. Advances in micro-crack studies have allowed their usage as representatives for larger scale fractures. The second approach takes statistical data for individual fracture attributes and pecifies their interdependence (i.e. power law distribution), describing the 3D fracture network as a whole (La Pointe and Hudson, 1985; Kulatilake et. al., 1993).
- Amplitude versus offset (AVO) analysis has proved to be useful for characterizing changes in material properties along a reflector. The AVO behaviour varies in fractured reservoirs due to fracture density, aspect ratio, and fluid saturation. Several studies mapped fractures or fracture properties as AVO anomalies (e.g. Schoenberg, 1995; Perez et al., 1999; Hall and Kendall, 2003; Hunt et al., 2010). This methodology requires pre-stack gathers for the study area, which are not always available.
- Microseismic technology allows recording of low-energy passive seismic or microseismic events that take place in the subsurface during drilling, stimulation and production. Microseismic mapping can accurately measure the hypocenters of acoustic emission associated with the changes in stress in the rock matrix (Sneddon, 1946), caused by the injection of fluids, gas, proppant, or other materials during the hydraulic fracture treatment or caused by other exploration or production activities. It yields a high degree of certainty in the direction, azimuth, height, length, and asymmetry of the hydraulic stimulation (Peterson et al., 1996). Microseismic techniques allow to predict details of fracture networks during and after treatment.

Procedures used for fracture network mapping are either spatially restricted (e.g. cores, geomechanics and image logs), rely on predictions from spatially restricted data (e.g. structural interpretation, and statistical approaches), or are based on post treatment measurements (e.g. microseismic). The only method that gives fracture mapping pre-drilling is AVO but with some uncertainties and the need of specific requirements (i.e. pre-stack gathers).

In this study we use seismic attributes, and in particular most-positive and ant tracking, to delineate fractures and small faults within shale intervals in the Cooper basin, which we then independently verified using image logs, cores, seismic amplitudes, and well data.

Geologic and Tectonic Setting of the Cooper Basin

The Cooper Basin is a Late Carboniferous to Middle Triassic basin located in the eastern part of central Australia (Fig. 1). The Cooper Basin floor was curved out of the uplifted topography following the formation of Warburton Basin. The sedimentary basins within the interior of the Australian continent have been subject to several tectonic events resulting in periods of subsidence, inversion, and uplift, from the Neoproterozoic until the present day (Preiss, 2000; Backé et al., 2010).

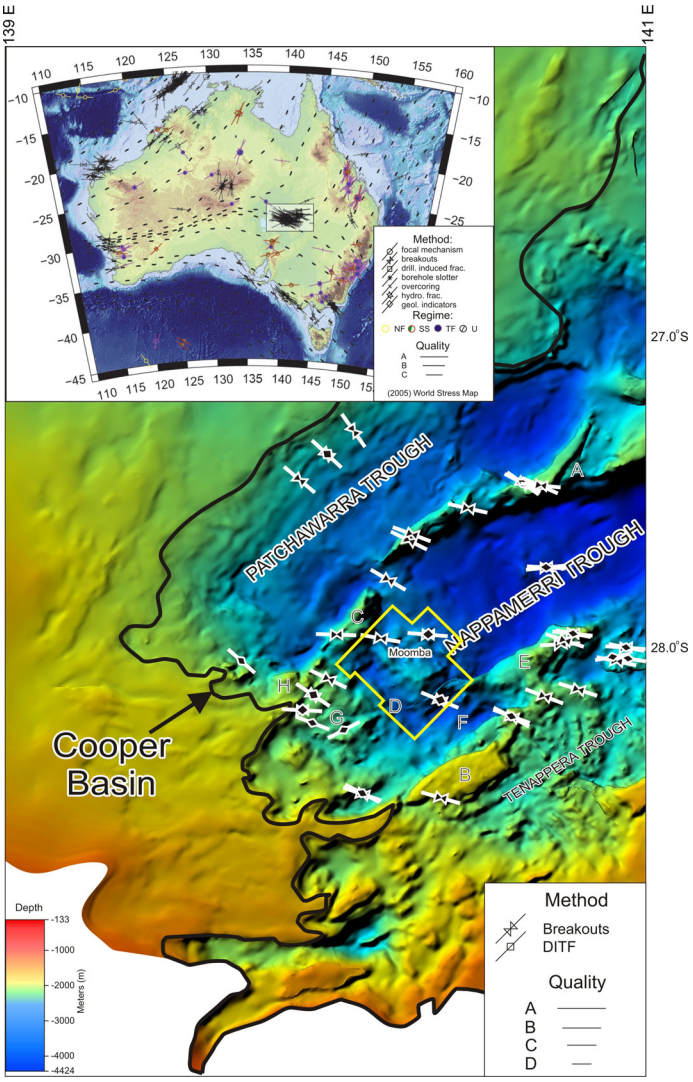

Figure 1. Top Warburton Basin (Pre-Permian Basement, seismic horizon Z) in the Cooper Basin (modified after the National Geoscience Mapping Accord (NGMA), 2009). Map shows NE-SW major troughs separated by ridges. Study area is located at the south-western termination of the Nappamerri trough (Moomba-Big Lake 3D seismic cube outlined in yellow). A: Innamincka Ridge; B: Murteree Ridge; C: Gidgealpa-Merrimelia Ridge; D: Wooloo Trough; E: Panoo Ridge; G: Della-Nappacoongee Ridge; F: Allunga Trough; H: Warra Ridge. Top left: Australian stress map (modified after Reynold et al, 2004; and The World Stress Map, 2010), Shmax (maximum horizontal stress direction) indicated in black lines.

Following the deposition of the Cambrian-Ordovician sequences of the eastern Warburton Basin underlying the Cooper Basin, NW-SE compression caused a partial inversion of the Warburton Basin, deformation of the pre-existing sequence and the subsequent intrusion of Middle to Late Carboniferous granites (Gatehouse et al., 1995; Gravestock and Flint, 1995; Alexander and Jensen-Schmidt, 1996). This tectonic event is coeval with the Alice Springs and Kanimblan Orogenies, which affected Central Australia.

The Early Permian sequences (Merrimelia, Tirrawarra and Patchawarra formations) were deposited in an environment largely controlled by Gondwanian glaciations (Powell and Veevers, 1987; Fig. 2). The depositional environment was comprised of high

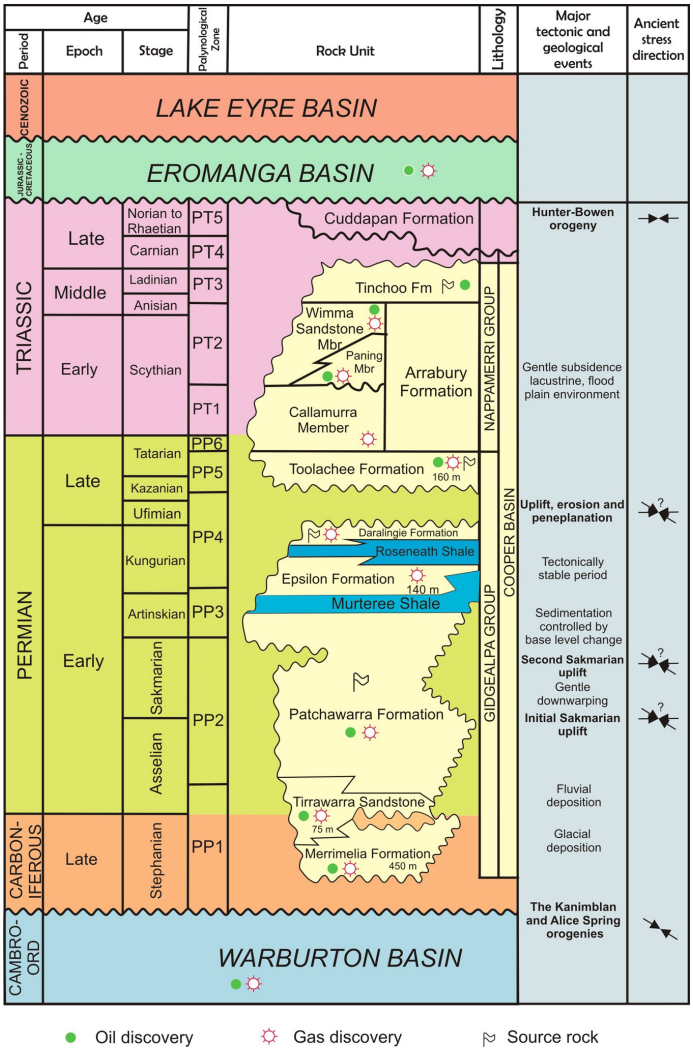

Figure 2. Stratigraphy and paleo-stress directions of the Cooper Basin (modified after PIRSA, 2010). The target shale layers are colored blue (Roseneath and Murteree shales).

sinuosity fluvial systems flowing northward over a floodplain with peat swamps, lakes and gentle uplands (Apak et al., 1997). The Patchawarra Formation constitutes the main conventional reservoir within the basin, and is intercalated with major coal seams in the basin (Apak et al., 1993, 1995, 1997).

The remaining Early Permian sequences (Murteree, Epsilon, Roseneath and Daralingie formations) were deposited during a period of tectonic quiescence, within an open basin environment with restricted access to the sea from the east (Stuart, 1976; Thornton, 1979). The latter sequences form the main target for shale gas exploration in the Cooper Basin. The final sequences of the Cooper Basin were deposited in the Late Permian in a period of tectonic quiescence, separated from the Early Permian sequences by the Daralingie Unconformity (Paten, 1969), in a meandering fluvial system (Tolachee Formation and Nappamerri Group). A basin-wide erosional unconformity marks the end of the Permo-Triassic Cooper Basin. That unconformity was caused by the Hunter-Bowen Orogeny (Wiltshire, 1982) which shifted the depocentre northwest and triggered the formation of Eromanga Basin.

Data and Methodology

This study focuses on the Moomba-Big Lake fields, which are located at the southwestern termination of the Nappamerri Trough (Figure 1). The fields are covered by a 3D seismic survey with an area of ~800 km^2 and contain around 300 oil and gas wells. Of these wells, twenty-nine wells have check shots (well bore seismic data used to measure the seismic travel time and P-wave velocityfrom surface to a known depth), that allow the seismic data interpretation to be tied to the geology. Furthermore, an additional 250 wells contain detailed geophysical wireline logs, four of which contain geophysical image logs, and a large number of wells have recorded drill stem tests (DST), repeated formation tests (RFT), leak off tests (LOT), and hydraulic fracture tests for depth intervals within and/or in the vicinity of the Roseneath and Murteree formations. The large amount of data available enables a detailed characterization of the fracture system in the Moomba-Big Lake fields.

Three horizons were interpreted (Murteree, Roseneath and Toolachee formations; Fig. 2) within the Moomba-Big Lake 3D seismic survey. Structural interpretation and structural basin models using seismic amplitudes and different seismic attributes were used to identify large-scale faulting trends and fractures network within the survey.

The orientations of the maximum horizontal stress (Shmax) and the minimum horizontal stress (Shmin) have been estimated using the interpretation of resistivity images of borehole walls produced by the Formation Micro Scanner (FMS) tool. In total, we interpreted 104 breakouts and 29 drilling induced tensile fractures (DITFs) from four wells with image logs in the Moomba-Big Lake seismic cube area.

We observed 139 natural fractures on the image logs with a combined length of 152m, that we tried to compare with observations from core data when available, and with the different attribute signatures obtained from seismic and well data at the same depths to gain confidence and for calibration.

Seismic Attributes

3D seismic attributes have proven to be amongst the most useful geophysical techniques for characterizing faults and fractures (Hakami et al., 2004; Chopra and Marfurt, 2007; Backé et al., 2011, Abul Khair, et al., 2012). 3D seismic volumes provide dense and regular sampling of data, and yield images that represent the areal extent of subsurface feature. One of the major advantages of 3D seismic is the ability to display 3D seismic volumes in vertical sections, horizontal time slices, and horizon time slices.

Among the hundreds of seismic attributes used in geophysical studies, structurally smoothed, non-steered attributes including most-positive curvature (MPC), most-negative curvature (MNC), and their ant tracks have proven most successful at delineating features that are mostly faults and/or fractures. We first created a structurally smoothed cube of the seismic events at every sample point from the seismic volume cube. Then, MPC and MNC attributes were calculated using the *Petrel* and *OpenDetect*™ software, while ant tracks were calculated using *Petrel* software. The target horizons (i.e. Murteree, Roseneath and Tolachee formation), were interpreted using *The Kingdom Suite*™, then the horizons were transferred to *Petrel* and *Opendtect* for attribute calculations.

Curvature Attributes

Fracture prediction using 3D seismic data is generally undertaken using seismic attributes such as curvature and different types of coherence (Hunt et al., 2010). Recent studies have investigated whether curvature attributes can provide an accurate and reliable prediction for fracture distributions and orientation, as well as permitting the definition of subtle faulting and fracturing patterns below seismic resolution (Hakami et al., 2004; Al-Dosary and Marfurt, 2006; Chopra and Marfurt, 2007; Abul Khair et al., 2012).

Curvature is defined as the reciprocal of the radius of a circle that is tangent to the given curve at a point (Chopra and Marfurt, 2007). An observed high value of curvature corresponds to curve, whereas curvature will be zero for a straight line (the same concept is applicable to surfaces). Using the curvature attribute enables mapping of geological structures, such as folds or faults, which are characterized by high curvature (positive or negative). From the different types of curvature attributes available to the seismic interpreter, the MPC attribute is able to successfully delineate upthrown fault blocks and crests of antiforms, whilst MNC attributes more successfully delineate the down-thrown faulted blocks of faults in addition to synclines (Chopra and Marfurt, 2007).

The MPC and MNC attributes permitted the delineation of subtle structural features that are interpreted as faults and fracture networks (Fig. 3). We carefully mapped these structures in order to define their trend and spacing, and to assess the reliability of using these complex curvature attributes for the definition of natural fractures (Fig. 4).

We recognized a primary trend for the faults and fractures that is oriented NW-SE, along with a secondary trend that is oriented NE-SW. These trends correspond to the primary and secondary structural trends in this region of the Cooper Basin (Fig. 4).

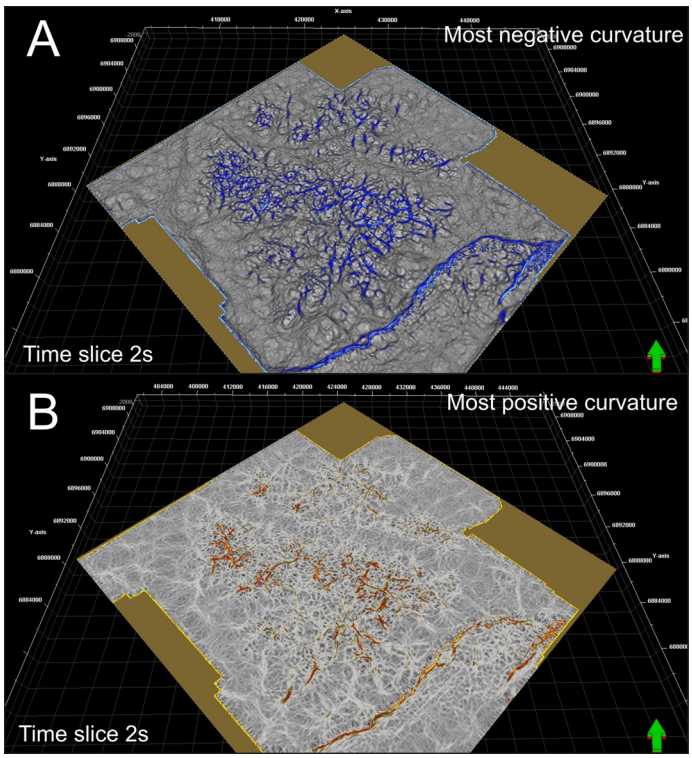

Figure 3. Most negative (A), and most positive (B) curvature attribute of the Moomba-Big lake fields. Features represent faults, accompanying large fractures, anticlines and synclines.

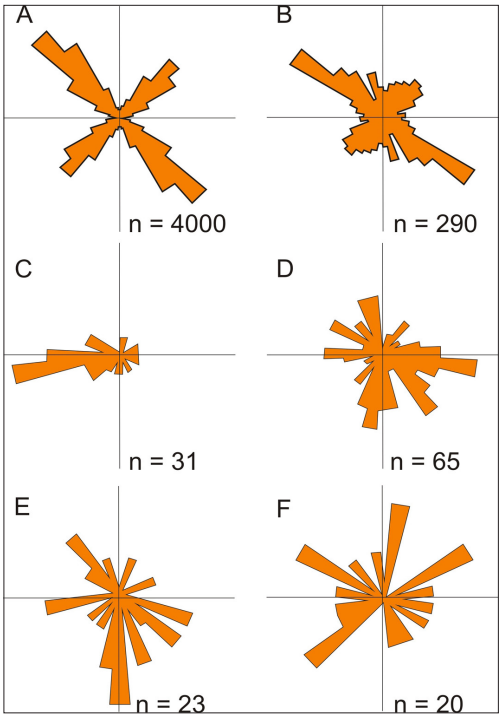

Figure 4. Rose diagram for the fracture networks measured in the Moomba-Big Lake field from A: curvature attributes, B: fault network, and from image logs in wells, C: Moomba 73, D: Big Lake 54, E: Moomba 78, F: Moomba 74.

Attribute Calibration

We used several types of calibration methods to check the validity of every type of attribute in order to map faults and fractures. These methods include image logs, seismic amplitudes, and well data control (i.e. observations of thickening and thinning of faulted and fractured layers).

Image Logs

Four wells within the Moomba-Big Lake fields have FMS images that encompass the depths of the shale formations (i.e. Roseneath and Murteree formations). We interpreted a total of 139 conductive and resistive fractures from these image logs. Conductive fractures are fractures that are open for fluid and gas circulation and appear on image logs as dark sinusoids, as they are filled with conductive drilling fluids. Resistive fractures appear on image logs as light sinusoids as they are filled with resistive cements (e.g. quartz, calcite). Rose diagrams of interpreted natural fractures in the four wells (Figs 4/C-F), display scattered strike directions for both conductive and resistive fractures, but the fractures appear to display a dominant NW-SE strike and a secondary NE-SW strike.

The comparison of fracture trends identified from FMS data and the complex seismic curvatures display a good correlation, with about 70% of the fractures mapped on the image logs corresponding to a high degree of curvature on both the most positive and most negative curvature maps, and with trends that are the same or parallel to the image logs fractures (Fig. 5).

We also conducted a core study in which we analyzed core samples held in the Primary Industries and Resources South

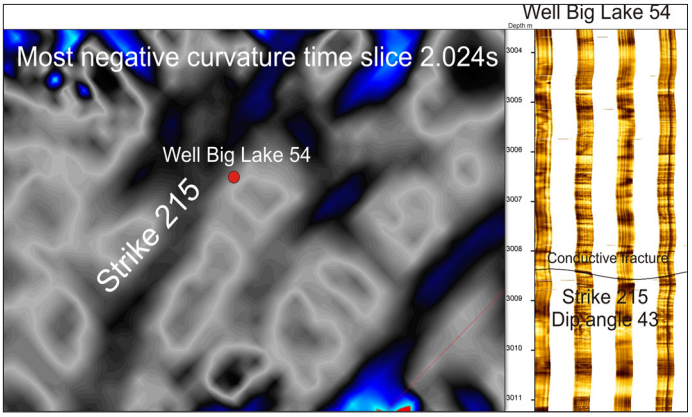

Figure 5. Formation micro scanner (right) for well Big Lake 54, showing a conductive fracture (Strike 215). Attributes calculated at the same depth show good curvature correlation.

Australia (PIRSA) store. Only three wells drilled within the Moomba-Big Lake seismic survey area contain cores over depths close to the interval of interest, but these do not have image logs to permit a direct correlation, and they are not oriented cores. We observed open fracture apertures as well as calcite or quartz cemented fractures.

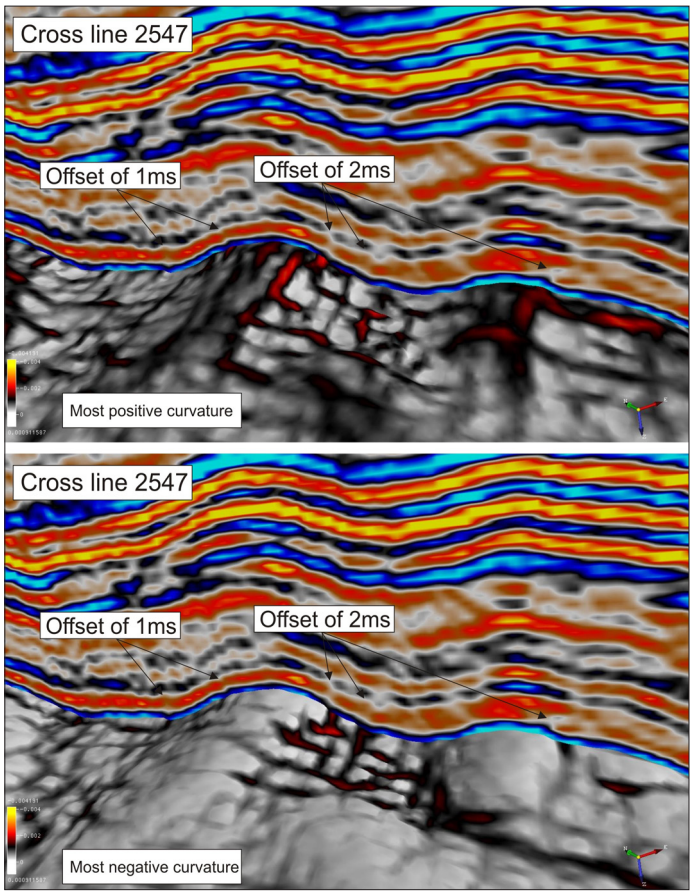

Figure 6. A chair display for seismic amplitude crossline 2547 from the Moomba-Big Lake cube displayed against most positive curvature attribute at calculated at Murteree shale (top photo), and most negative curvature attribute at the Murteree shale (bottom photo).

Seismic Amplitudes

The use of 3D seismic amplitude surveys represents the most powerful and accurate tool for studying large subsurface structures such as faults and folds. However, because fractures are generally below the seismic resolution of any seismic volume, direct analysis of the seismic amplitude cross-sections cannot be used to identify and map fracture networks. We studied closely the amplitude signatures displayed on the inlines and crosslines that show fault offsets, and carefully compared them with attribute signatures to determine whether or not seismic attributes can map faults with small offsets, and to which degree of resolution and accuracy.

We calculated curvature attributes at the top of the shale horizons (i.e. Murteree and Roseneath formations), and compared the attribute signature with every inline and crossline (Fig. 6). The MPC and MNC attributes succeeded in mapping faults with offsets as small as 1 ms (Fig. 6).

In order to determine the threshold of the curvature values that reflect small fault offsets or fold structures, we conducted a statistical study of the values of the curvature signatures which we compared to the structures mapped at the seismic amplitude cross sections. Four types of seismic amplitude features could be mapped by the curvature signatures (faults, folds, micro-folds, and unstructured features) (Table 1). A total of 21.7% of the curvature signatures did not correlate to any apparent structural feature. The average curvature values of this part is 0.09. Thus, when considering curvature attributes for fault mapping, weak curvature signatures up to 0.2 should be eliminated from the survey. These weak signatures might reflect the fracture network within the survey, but lack of reasonable number of wells containing image logs made it hard to prove that. A detailed study made by Abul Khair et al. (2012), showed that curvature signatures at the depth of the fractures mapped on image logs show good correlation.

Table 1. Statistical study for the most positive curvature signatures in the Moomba-Big Lake fields.

	Faults	Anti-clines	Micro-anticlines	No Structure
No. of samples	63	49	55	46
Average curvature value	0.43	0.46	0.23	0.09
Minimum curvature value	0.14	0.18	0.06	0.03
Maximum curvature value	0.99	0.99	0.58	0.17
Percentage	29.5%	23%	25.8%	21.7%
Standard deviation	0.22	0.22	0.11	0.03

Well Data

Because faults variably affect formation thicknesses, according to their sense of offset, we also used stratigraphic variations to determine the existence of small faults cutting wells, and to compare these faults with attribute signatures. Two flooding surfaces (FS) were picked and mapped within the Roseneath Formation for all wells containing geophysical logs in the Moomba-Big Lake fields (i.e. SC00 and SC70; Fig. 7). These FS were picked based on signatures in gamma ray, sonic and resistivity logs. The thicknesses of six zones, shown in figure 7, within Roseneath Formation were calculated and a grid was created for the thicknesses in order to locate extant "Bulls

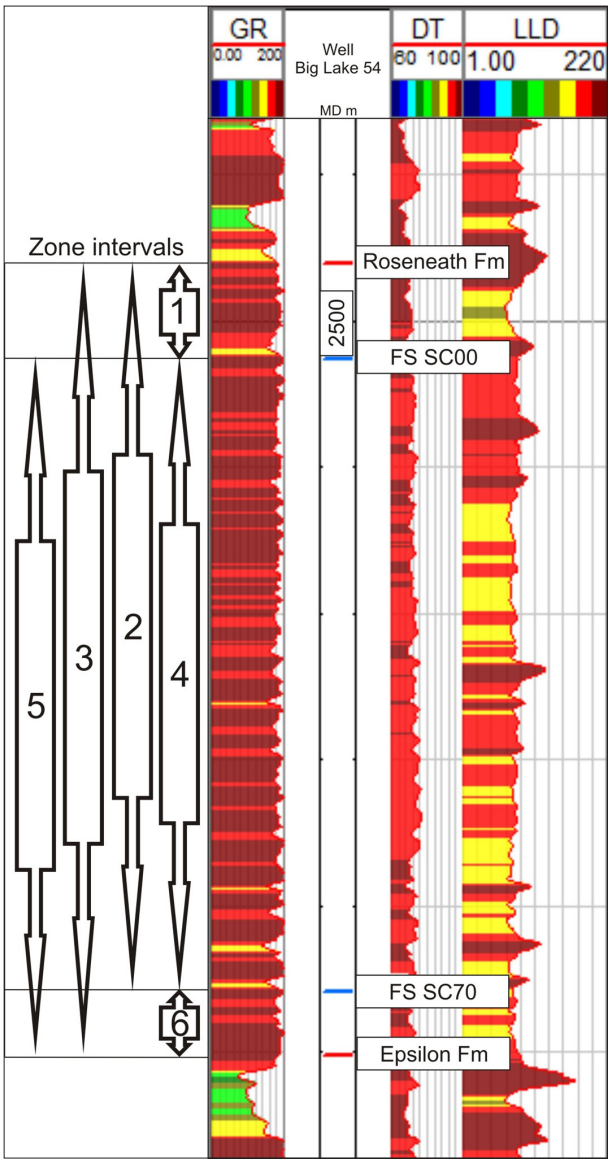

Figure 7. Zones (1-6) within Roseneath Formation in the Moomba-Big Lake fields used to compare thickness with the attribute signature as indicator of thickening or thinning resulted from faulting.

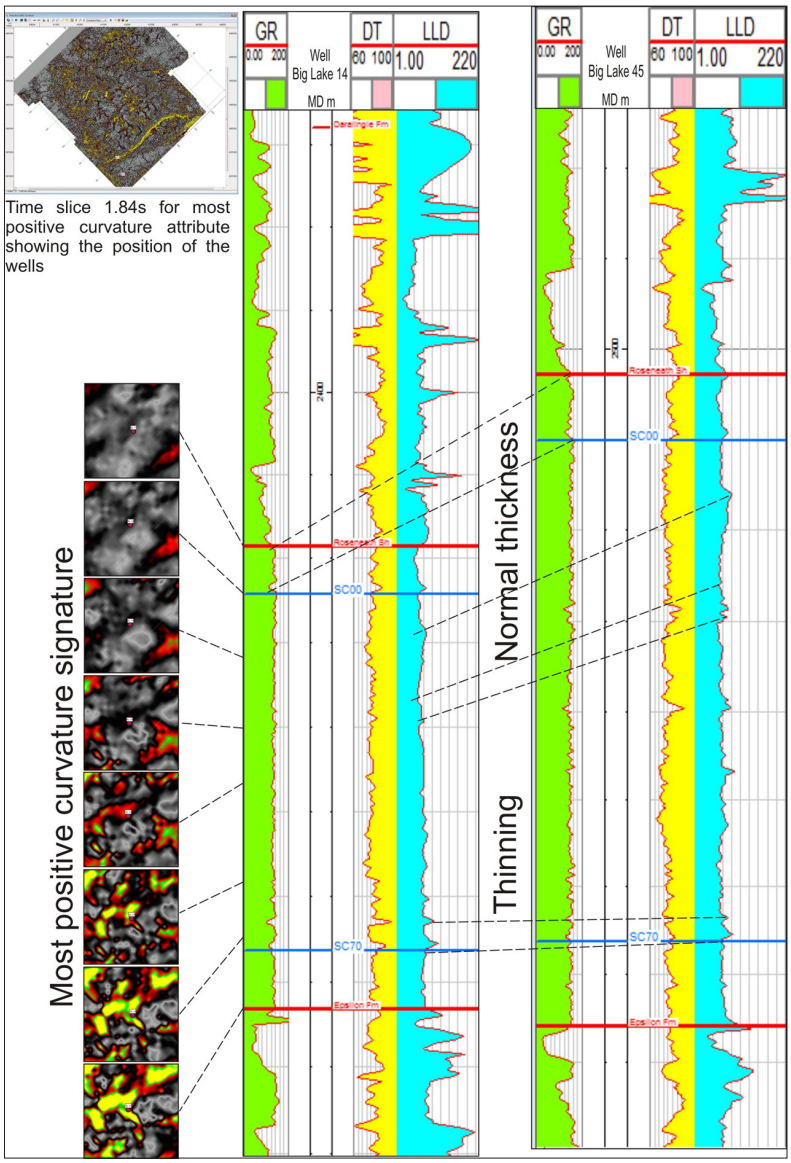

Figure 8. Well Big Lake 14 shows thinning against well Big Lake 45. Note that thinning exists in the lower half of the formation and is reflected by high curvature values.

Eyes", an expression indicating local thickening or thinning that may be related to faulting.

Any change in the thickness of a zone within a well can be a result of lateral lithological changes or fault cutting the well. Lateral changes in the formation thickness can be recognized from seismic amplitude crosslines and inlines. Faults with small offsets, below the seismic resolution, will cause thickness changes and will be only mapped by seismic attributes.

Normal faults that offset wells will cause loss of layers (thinning of the studied zones), while reverse or thrust faults that cut wells will cause repetition of the layers (thickening of the studied zone). The thickness maps were studied carefully, and whenever a change in the thickness of any of the zones was identified, the seismic amplitude cross section was checked for any lateral changes. If the seismic amplitude showed no lateral changes, the most positive curvature attribute map was displayed to check the existence of any signature that might reflect small faults (Fig. 8).

More than 80% of the thickness variations that are not caused by lateral lithological changes are found to display high values of curvature signature (Fig. 8). This indicates that the most positive curvature attribute succeeded in mapping small faults that are not mapped by seismic amplitude. Thus, these faults can be considered as representative for the fractures as they are below seismic amplitude resolution.

Eliminating Undesired Curvature Values

It has been found, from using all the calibration methods for checking the validity of the curvature attribute to map faults and

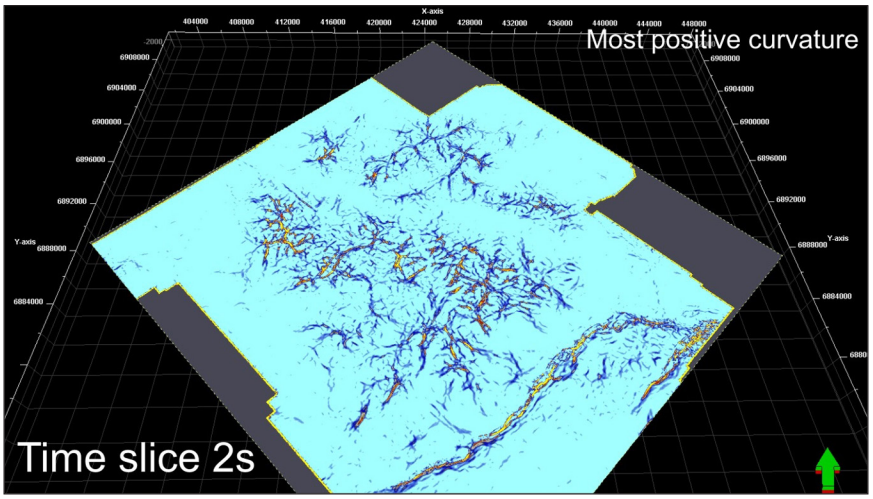

Figure 9. Most positive curvature attribute calculated after eliminating the values less or equal to 0.2.

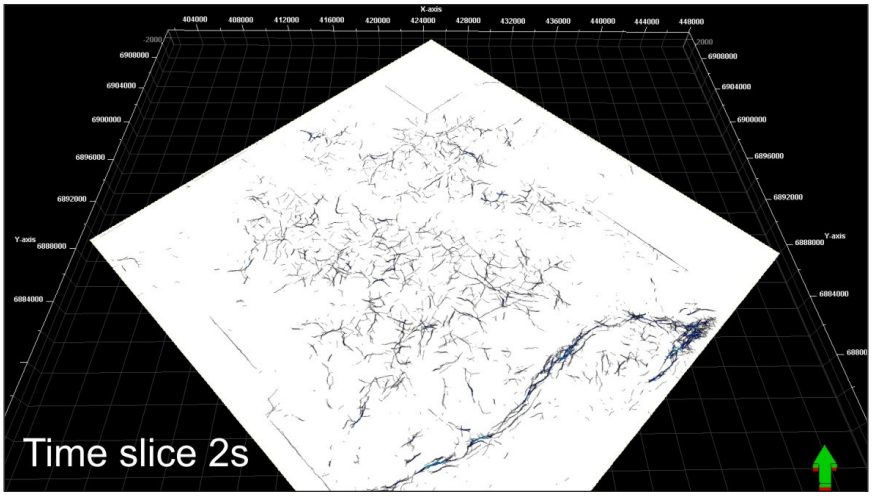

Figure 10. Ant tracking processed for the most positive curvature attributes generated after eliminating the undesired vales.

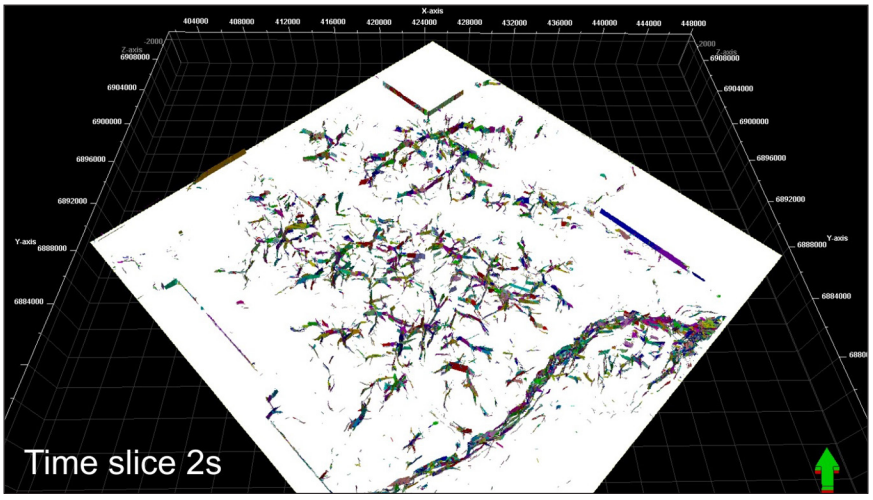

Figure 11. Automatic fault and fracture extraction using the ant tracks signatures.

fractures, that the curvature values less than 0.2 are not mapping any structural features. Thus, a new seismic curvature cube was created with all the values more than 0.2 for better mapping the faults and folds (Fig. 9).

Ant Tracking

Several recent studies have used ant tracking methodologies for fast extraction of fault networks. The algorithm employed by this attribute follows an analogy of the behavior of ants, as they choose the shortest path between their nest and food using pheromones for communications. As the shortest path will be marked with more pheromones, next ant is more likely to choose the shortest route, and so on. During the process, a large number of electronic ants are distributed in the seismic volume allowing them to move along faults and emitting pheromones. Surfaces that are strongly marked with pheromones are likely to be faults (Randen et al., 2001; Fehmers and Hocker, 2003; Skov et al., 2003; Aguado et al., 2009; Fig. 10).

The ant tracking process allows the user to define some variables during the procedure. In order to define all the discontinuities within the Moomba-Big Lake seismic volume, the variables were set for the ants to track any variation between the seismic signals within three step points for each increment of its search. The initial ant boundary, which controls how closely the initial ant agents can be placed within the volume, was chosen so that more details will be captured. Thus, all the variables were chosen to achieve the highest details about the discontinuities.

Automatic Fault and Fracture Extraction

The automatic fault extraction process provides an interactive tool for extracting fault patches from an edge volume. This tool is used these days for fast 3D mapping of faults using specific types of attributes capable to map structural edges.

In this study, we applied the automatic fault extraction tool for the ant tracks cube calculated from the most positive curvature cube after eliminating the undesired values. We applied an aggressive algorithm that will 3D map all the available structural features mapped by the ant tracks (Fig. 11).

In-Situ Stress Orientations and Magnitudes

We used borehole breakouts and DITF's observed on image logs to determine orientations of the three principal stresses. In the Earth's crust, the three principal stresses can be resolved in to a vertical and two horizontals stresses (Anderson,

1951). The vertical stress is assumed to be vertical. The horizontal stresses lie in a plane 90° degrees from vertical (Zoback, 2007).

When the circumferential stress acting around a wellbore exceeds the compressive strength of the rock in a vertical well, conjugate shear fractures form at the wellbore wall centred on the minimum horizontal stress direction, causing the rock to spall off (Bell & Gough 1979). As a result, the wellbore becomes enlarged in the minimum horizontal stress direction, which forms the wellbore breakouts. Borehole breakouts form perpendicular to the present-day Shmax orientation and appear on image logs as dark conductive areas separated by 180° (Kirsch, 1898; Bell, 1996).

DITF's form parallel to the present-day Shmax in vertical wells and appear on image logs as dark conductive fractures separated by 180 °. DITF's are different from pre-existing natural fractures in many characteristics. On image logs, DITF's are not longer than 2 m, often contain small jogs or kinks, discontinuous, and appear as dark, electrically conductive fractures. Whereas, natural fractures appear as continuous sinusoids, and can be conductive or resistive (Barton and Zoback, 2000). Both borehole breakouts and DITF's appear on image logs separated from each other by 90 °. Our analyses of the interpreted 104 breakouts and 29 drilling induced tensile fractures show a consistent Shmax direction trending at N101 ° E (Table 2). This is consistent with a previous basin-wide study conducted by Reynolds et al., (2004), which gave a Shmax orientation of N 101°, as interpreted from compiled data across the whole of the Cooper Basin.

Table 2. Number of borehole breakouts and drilling-induced tensile fractures recorded in each well. Quality ranking is according to World Stress Map Criteria (Heidbach et al., 2010).

Borehole Name	n	Total Length (m)	Shmax Orientation	S.D.	Quality
Big Lake 54	67	64	104° N	5.5°	B
Moomba 73	31	35	97° N	6.5°	C
Moomba 74	7	11	101° N	3°	D
Moomba 78	28	42	97° N	5.3°	B

The magnitude of Sv at any depth within the crust is equivalent to the pressure exerted by the weight of the overlying rocks (Engelder, 1993; equation 1).

$$Sv = \int_0^z \rho(z) g \, dz \qquad (1)$$

We calculate the magnitude of Sv using density logs when available, and interval velocities when density logs were not available. The magnitude of Shmin, is estimated from hydraulic fracture tests and leak off tests. The lower bound of the leak-off pressure is considered to provide a reasonable estimate of the minimum horizontal stress (e.g. Breckels & van Eekelen 1982; Bell 1996). The upper bound to the magnitude of the maximum horizontal stress, is constrained by assuming that the ratio of the maximum to minimum effective stress cannot exceed that

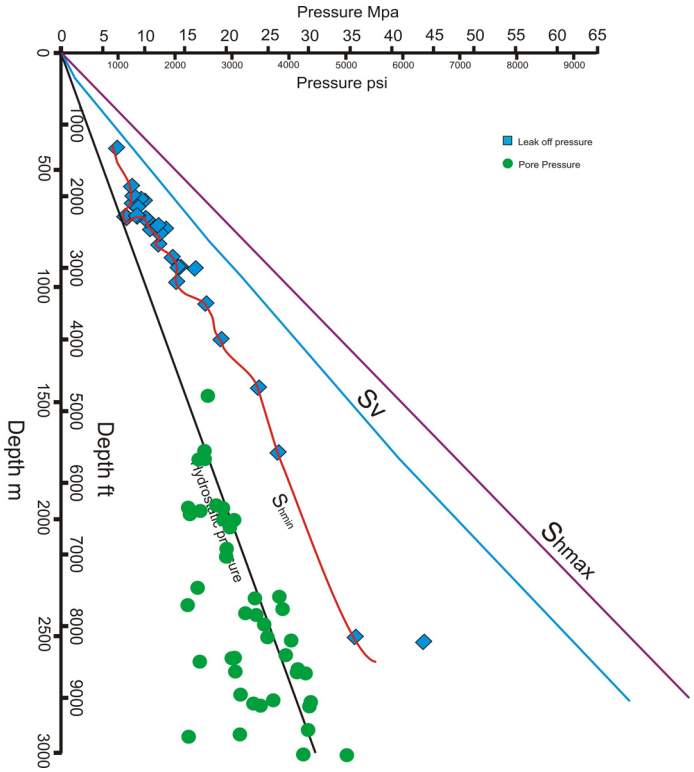

Figure 12. Stress magnitude verse depth plot of the Moomba-Big Lake fields. Sv: vertical stress, Shmax: maximum horizontal stress, Shmin: minimum horizontal stress.

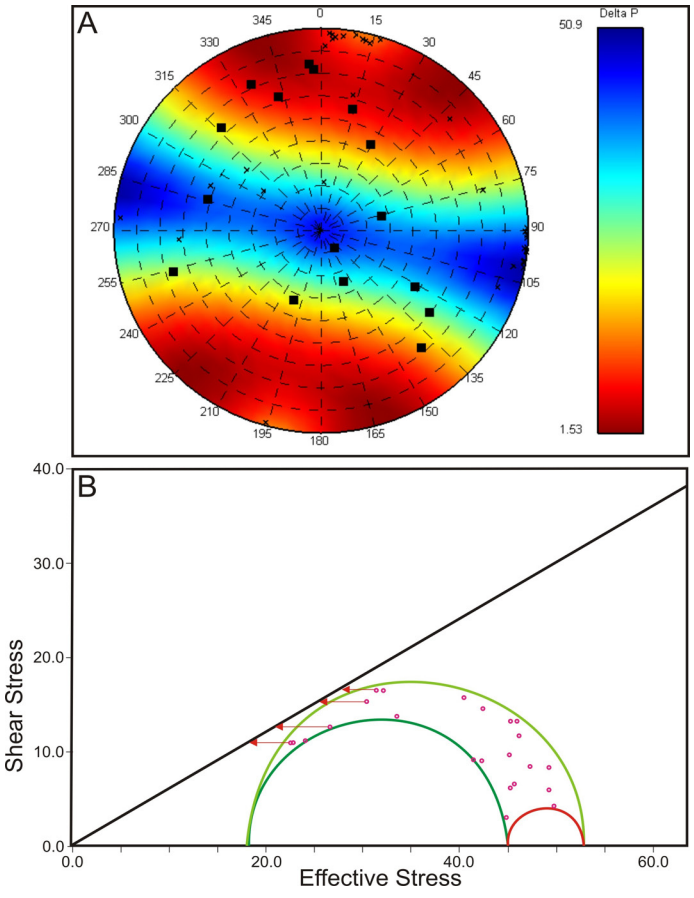

Figure 13. Structural permeability stereonet (A) and mohr diagram (B) for well Moomba 78 at the depth of Murteree shale in the Moomba-Big Lake fields.

required to cause faulting on an optimally oriented pre-existing fault (Sibson 1974).

The calculated magnitudes of the three principle stresses in the Moomba-Big Lake fields resulted that, Shmax was found to be the higher principle stress, and the magnitude of the vertical stress was found to be greater than the minimum horizontal stress, indicating that a strike-slip stress regime (Shmax > Sv > Shmin) dominates the field (Fig. 12). This result is consistent with the earlier findings of Reynolds et al. (2004).

Fracture stimulation conducted in fields with strike-slip stress regimes allows the formation of a conjugate set of fractures with a trend 30° from Shmax (Zoback, 2007). The Shmax orientation has been measured at N101 °E, thus, new fractures will open during stimulation as conjugate sets striking approximately N071 °E and N131 °E.

Fracture Susceptibility

The determination of fracture susceptibility requires a detailed knowledge of the in-situ stress field and pre-existing fracture orientations (Reynolds et al., 2004; Zoback, 2007). Fractures that are optimally oriented for reactivation within the in-situ stress field will have higher permeability than fractures that are not (Barton et al. 1995; Finkbeiner et al. 1997). In this study, we used the JRS software to calculate the fracture susceptibility since it uses shear and tensile modes of failure and provides a measure of the required increase of pressure to induce failure. This software uses the stress tensor (3D Mohr circle) and rock strength (failure envelope). All the fractures are plotted within the 3D Mohr circle, and those closer to the failure envelope are most likely to open during stimulation (Fig. 13). The horizontal distance between each fracture in the Mohr circle and the failure envelope represents the pressure increase required to initiate failure.

We generated Mohr diagrams and structural permeability stereonets for the horizons of interests for each of the four wells, where image logs were available (Fig. 13). The structural permeability stereonets show that fractures striking between N140 °E and N250 °E are more likely to reactivate during fracture stimulation. Fractures with highest susceptibility, closer to the failure envelope, strike between N155 °E and N170 °E, and between N210 °E and N225 °E.

Discussion and Conclusions

Application of most positive and most negative curvature seismic attributes and its ant tracks to Permian shale gas and geothermal energy exploration targets in the Cooper Basin delineate structural features that are similar in geometry to fracture networks. Comparing these features with fractures observed on image logs and the mapped fault network indicated that around 80% of these features are always parallel to them. It is believed that the attributes features with high values we identify are mostly large and small faults, and that fractures we have interpreted in image logs are fractures located within the damage zones of these faults.

Well control checks using the effect of faults on thickening and thinning of specific stratigraphic intervals showed that the majority of thickness change, which is not caused by lateral sedimentological changes, display strong curvature signatures. Thus, values of specific curvature attributes might be used with high confidence to differentiate between large and small faults, which will reflect, to a certain degree, the fracture network.

The in-situ stress field determined for the Moomba-Big Lake fields indicate a strike-slip stress regime with the Shmax orientation at N101°E. Fracture stimulation programs under this stress regime will cause the formation of a conjugate set of fractures that strike 30° from Shmax, approximately N071 °E and N131 °E. As the dominant fault and fracture networks trend NW-SE and NE-SW, it is most likely that the pre-existing set of fractures will open depending on their susceptibility. A fracture susceptibility study conducted for the shale intervals in the Moomba-Big Lake fields indicates that the major fault and fracture network trends (i.e. NW-SE and NE-SW) are highly susceptible for reactivation under present-day stress regime in the basin. Mohr circles show that very small increase in pore pressure (i.e. 2 MPa in some cases) is required for these fractures to reach failure. This is one of the main reasons behind the availability of the fractures within the shale intervals.

Finally, the methodology used in this study provided the stages of the workflow required for mapping subsurface fracture networks (Figure 14):

1. Seismic conditioning: during this stage, structural smoothing filters should be applied to the seismic volume to eliminate noise and artifacts.
2. Edge detection: two attributes can be used and applied for the seismic volume (i.e. most positive and most negative curvature). As these attributes are considered edge attributes, they should be able to map small faults and fractures.
3. Eliminating curvature values less or equals 0.2 of the volume in order to map only structural features.

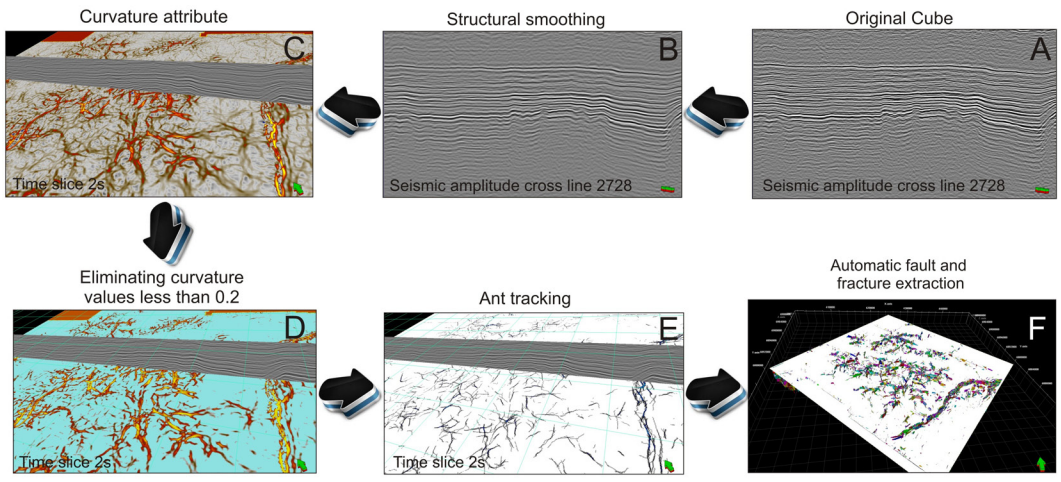

Figure 14. Data analysis workflow to map and 3D modeling the orientation, density, and spatial distribution of subsurface fracture networks.

4. Edge enhancement: electronic ants should be distributed within the seismic volume to map faults.
5. Interactive interpretation (surface extraction): a collection of surface segments and fault patches eventually extracted from the ant track attribute.
6. Calculating the in situ stress field direction and magnitude, and determining fracture susceptibility.

Acknowledgments

The authors would like to acknowledge the appreciated financial contribution and provision of the data from the Petroleum and Geothermal division of Primary Industries and Resources SA. In particular, the help of Barry Goldstein, Tony Hill and Elinor Alexander were really appreciated, and The South Australian Centre for Geothermal Energy Research (SACGER). Many thanks to the generous donation of Academic Licenses of OpenDetect™ from dGb Earth Sciences, The Petrel Suite from Schlumberger, The Kingdom Suite™ from Seismic Micro Technologies and JRS Image Log Interpretation Suite from JRS Petroleum Research.

References

Abul Khair H., G. Backé, R. King, S. Holford, M. Tingay, D. Cooke, and M. Hand, 2012. "Factors influencing fractures networks within Permian shale intervals in the Cooper Basin, South Australia." APPEA 2012 conference.

Aguado D.B., A. Kaschaka, and L.F. Pinheiro, 2009. "Seismic Attributes in Hydrocarbon Reservoirs Characterization", Universidade de Aveiro, pp 165.

Al-Dosary S., and K.J. Marfurt, 2006. "3-D volumetric multi-spectral estimates of reflector curvature and rotation": *Geophysics*, **17**, no.5, p41-45.

Alexander E.M. and B. Jensen-Schmidt, 1996. "Structural and Tectonic history." In: The petroleum Geology of South Australia, Volume 2: Eromanga Basin. Petroleum Division, SA Department of Mines and Energy, Report Book, 96/20.

Anderson E. M., 1951. "The Dynamics of Faulting and Dyke Formation with Applications to Britain." Edinburgh, Oliver and Boyd.

Apak S.N., W.J. Stuart, and N.M. Lemon, 1993. "Structural stratigraphic development of the Gidgealpa.Merimelia.Innamincka Trend with implications for petroleum trap styles, Cooper Basin, Australia." *APEA Journal,* 33:94-104.

Apak, S.N., W.J. Stuart, and N.M. Lemon, 1995. "Compressional control on sediment and facies distribution, SW Nappamerri Syncline and adjacent Murteree High, Cooper Basin." *APEA Journal,* 35(1):190-202.

Apak, S.N., W.J. Stuart, N.M. Lemon, and G. Wood, 1997. "Structural evolution of the Permian.Triassic Cooper Basin, Australia: relation to hydrocarbon trap styles." *AAPG Bulletin,* 81(4):533-554.

Backé G., H. Abul Khair, R. King, and S. Holford, 2011. Fracture mapping and modelling in shale-gas target in the Cooper basin, South Australia, *APPEA*, accepted.

Backe, G., G. Baines, D. Giles, W. Preiss, and A. Alesci, 2010. "Basin geometry and salt diapirs in the Flinders Ranges, South Australia: Insights gained from geologically-constrained modelling of potential field data." *Marine and Petroleum Geology*, doi:10.1016 / j. marpetgeo. 2009.09.001.

Barton, C. A., and M.D. Zoback, 2000. "Discrimination of natural fractures from drilling-induced wellbore failures in wellbore image data-implications for reservoir permeability." SPE Reservoir Evaluation and Engineering 5, 249-254.

Barton, C.A., M.D. Zoback, and D. Moos, 1995. "Fluid flow along potentially active faults in crystalline rock." Geology, v. 23, 683–686.

Bell, J.S., 1996. "Petro Geoscience 2, in situ stresses in sedimentary rocks (part 2): applications of stress measurements", Geoscience Canada, **23,** 135–153.

Bell, J.S., and D.I. Gough, 1979. "Northeast-southwest compressive stress in Alberta: Evidence from oil wells": Earth and Planetary Science Letters, v. 45, p. 475-482.

Breckels, I.M., and H.A.M. Van Eekelen, 1982. "Relationship between horizontal stress and depth in sedimentary basins." Journal of Petroleum Technology, v. 34, 2,191–2,198.

Chopra, S., and K. Marfurt, 2007. "Volumetric Curvature Attributes adding value to 3D seismic data interpretation"; The Leading Edge, 26, 856-867.

Engelder, T., 1993. "Stress Regimes in the Lithosphere": Princeton University Press.

Fehmers, G.C., and C.F. Hocker, 2003. "Fast structural interpretation with structure-oriented filtering." Geophysics, vol. 68, no. 4, p. 1286-1293.

Finkbeiner, T., C.A. Barton, and M.D. Zoback, 1997. "Relationships among in situ stress, fractures and faults, and fluid flow: Monterey Formation, Santa Maria Basin, California." AAPG Bulletin, v. 81, 1,975–1,999.

Gatehouse, C.G., C.M. Fanning, and R.B. Flint, 1995. "Geochronology of the Big Lake Suite, Warburton Basin, northeastern South Australia." South Australia. Geological Survey. Quarterly Geological Notes, 128:8-16.

Gravestock, D.I. and R.B. Flint, 1995. "Post-Delamerian compressive deformation. In: Drexel, J.F. and Preiss, W.V. (Eds), The geology of South Australia. Vol. 2, The Phanerozoic. South Australia. Geological Survey. Bulletin, 54, 60–1.

Hakami, A., K. Marfurt, and S. Al-Dossary, 2004, "Curvature attribute and seismic interpretation: Case study from Fort Worth Basin", Texas, USA, SEG Expanded Abstracts, 23, 544.

Hall, S.A. and J.M. Kendall, 2003. "Fracture characterization at Valhall: Application of P-wave amplitude variation with offset and azimuth (AVOA) analysis to a 3D ocean-bottom data set." Geophysics, 68(4):1150-1160.

Heidbach, O., M.R.P. Tingay, A. Barth, J. Reinecker, D. Kurfeβ, and B. Müller, 2010. "Global crustal stress pattern based on the 2008 World Stress Map database release." Tectonophysics 482, 3–15.

Hunt, L., S. Reynolds, T. Broen, and S. Hadley, 2010. "Quantitative estimate of fracture density variations in the Nordegg with azimuthal AVO and curvature: A case study", The Leading Edge, 1122-1137.

Kirsch, V., 1898. "Die Theorie der Elastizität und die Beddürfnisse der Festigkeitslehre": Zeitschrift des Vereines Deutscher Ingenieure, v. 29, p. 797-807.

La Pointe, P.R. and J.A. Hudson, 1985. „Characterization and Interpretation of Rock Mass Joint Patterns", Geological Society of America Special Paper 199, 37.

Lyakhovsky, V., 2001. "Scaling of Fracture Length and Distributed Damage," Geophysical Journal International **144**, 114-122.

Olson, J. and D.D. Pollard, 1989. "Inferring paleostresses from natural fracture patterns: A new method," Geology **17**, 345-348.

Olson, J. E., Y. Qiu, J. Holder, and P. Rijken, 2001. "Constraining the spatial distribution of fracture networks in naturally fractured reservoirs using fracture mechanics and core measurements" 2001 SPE Annual Technical Conference and Exhibition.

Paten, R.J., 1969. "Palynologic contributions to petroleum exploration in the Permian formations of the Cooper Basin, Australia." APEA Journal, 9(2):79-87.

Pérez, M.A., R.L. Gibson, and M.N. Toksöz, 1999. "Detection of fracture orientation using azimuthal variation of p-wave avo responses." Geophysics, 64(4):1253-1265.

Peterson, R.E., S.L. Wolhart, K.H. Frohne, N.R. Warpinski, P.T. Branagan, and T.B. Wright, 1996. "Fracture diagnostics research at the GRI/DOE Multi-Site project: overview of the concept and results", SPE 36449, 1996 SPE Annual Tech. Conf. and ExhibitionDenver, CO, pp. 315–326.

Powell, C., and J.J. Veevers, 1987. "Namurian uplift in Australia and South America triggered the main Gondwanan glaciation." Nature, 326:177-179.

Preiss, W.V., 2000. "The Adelaide Geosyncline of South Australia and its significance in Neoproterozoic continental reconstruction," Precambrian Research, 100, 21–63.

Randen, T., S. Perdensen, L. Sonneland, 2001. "Automatic Extraction of Fault Surfaces from Three-Dimensional Seismic Data, Ann. Internat. Mtg., Soc. Expl. Geophys.. Expanded Abstracts.

Reynolds, S.D., S.D. Mildren, R.R. Hillis, and J.J. Meyer, 2004. "The in situ stress field of the Cooper Basin and its implications for hot dry rock geothermal energy development": PESA Eastern Australian Basins Symposium II, p. 431-440.

Rives, T., M. Razack, J.P. Petit, and K.D. Rawnsley, 1992. "Joint Spacing: "Analogue and Numerical Simulations," Journal of Structural Geology 14, No. 8/9, 925-937.

Schoenberg, M. and C.M. Sayers, 1995. Seismic anisotropy of fractured rock. Geophysics, 60(1):204-211.

Sibson, R.H., 1974. "Frictional constraints on thrust, wrench and normal faults." Nature, v. 249, 542–544.

Skov, T., T. Perdensen, T. Valen, P. Fayemendy, A. Gronlie, J. Hansen, A. Hetlelid, T. Inversen, T. Randen, and L. Sonneland, 2003. "Fault Systems Analysis Using a New Interpretation Paradigm": EAGE 65th Conference & Exhibition-Stavanger, Norway, 2-5 June.

Sneddon, I.N., 1946. "The distribution of stress in the neighbourhood of a crack in an elastic solid." Proc. Royal Soc. Lond., Ser. A, 187 (1946), pp. 229–260.

Stuart, W.J., 1976. "The genesis of Permian and lower Triassic reservoir sandstones during phases of southern Cooper Basin development." APEA Journal, 16:37-47.

Thornton, R.C.N., 1979. "Regional stratigraphic analysis of the Gidgealpa Group, southern Cooper Basin, Australia." South Australia. Geological Survey. Bulletin, 49.

Wiltshire, M.J., 1982. "Late Triassic and Early Jurassic sedimentation in the Great Artesian Basin." In: Moore, P.S. and Mount, T.J. (Compilers), Eromanga Basin Symposium, Adelaide, 1982. Summary papers. Petroleum Exploration Society of Australia, Geological Society of Australia (SA Branches), pp.58-67.

Zoback, M., 2007. "Petroleum Geomechanics." Cambridge University Press, 464, ISBN: 978052177069.